RSC Advances

PAPER

View Article Online
View Journal | View Issue

Cite this: *RSC Adv.*, 2023, **13**, 34358

Magnetoplasmonic photonic arrays for rapid and selective colorimetric detection of chloride ions in water†

Van Tan Tran, *[a] Van-Duong Dao, [a] Huu-Quang Nguyen, [b] Lemma Teshome Tufa,[b] Jaebeom Lee, [b] Van-Tuan Hoang *[c] and Anh-Tuan Le *[c]

The rapid and efficient detection of chloride (Cl^-) ions is crucial in a variety of fields, making the development of advanced sensing methods such as colorimetric sensors an imperative advancement in analytical chemistry. Herein, a novel, selective, and straightforward paper-based colorimetric sensing platform has been developed utilizing an amorphous photonic array (APA) of magnetoplasmonic Ag@Fe_3O_4 nanoparticles (MagPlas NPs) for the detection of Cl^- in water. Taking advantage of the highly responsive APA, the key principle of this sensing method is based on the chemical reaction between Ag^+ and Cl^-, which results in the precipitation of high-refractive index (RI) AgCl. This assay, distinct from typical plasmonic sensors that rely heavily on nanoparticle aggregation/anti-aggregation, is premised on the precipitation reaction of Ag^+ and Cl^-. In the presence of Cl^-, a rapid, distinctive color alteration from royal purple to a dark sky blue is visually observable within a short time of a few minutes, eliminating the necessity for any surface modification procedures. Comprehensive assessments substantiated that these sensors display commendable sensitivity, selectivity, and stability, thereby establishing their effective applicability for Cl^- analysis in various technological fields.

Received 5th October 2023
Accepted 18th November 2023

DOI: 10.1039/d3ra06754h

rsc.li/rsc-advances

1. Introduction

While halide ions are essential for proper physiological functions in the human body, their excessive presence can lead to various health complications.[1] Specifically, the chloride ion (Cl^-) represents a principal anion with significant implications across diverse fields. However, excessive concentrations of Cl^- can lead to hypertension and other cardiac diseases.[2] Although elevated levels of Cl^- in the environment may not directly impact human health, they can induce significant corrosion in metal pipes. Moreover, monitoring Cl^- ion concentrations (C_{Cl}) in sweat can provide an in-depth understanding of sweat composition, consequently ascertaining the physiological status of an individual.[3] Therefore, it is crucial to detect Cl^- in drinking water, the environment, and sweat in the current context. Several analytical methods have been documented for Cl^- detection, encompassing ion chromatography,[4] electrochemistry,[5] spectrophotometry,[6] and colorimetry.[7] Among these, the spectroscopic procedure involving mercury(II) salt is widely adopted and is endorsed by the Association of Official Analytical Chemists as the standard approach for Cl^- determination in natural water.[8] However, this method's primary limitations include the use of a highly toxic and expensive reagent, a time-intensive process, and costly equipment, which are impractical for routine operations and on-site monitoring. Consequently, there is a growing need to develop a greener, simpler, and more cost-effective alternative method that minimizes the use of hazardous reagents and reduces toxic waste generation.

The importance of colorimetric analysis has significantly escalated in recent years, bolstering the operational efficiency of plasmonic and photonic-based sensors.[9–13] Notably, noble metal NPs, including silver (Ag) and gold (Au) NPs, owing to their unique properties such as operational simplicity, cost-effective production, sensitivity, and straightforward construction, have been extensively employed in colorimetric sensors due to the method's sensitive and selective detection capability.[14–16] Nonetheless, the integration of nanoparticles onto support materials often necessitates a combination with supplementary technologies to amplify signals through optical, magnetic, or electrochemical readers. Alternatively, colorimetric sensing strategies that harness the structural color of photonic crystals (PCs) to generate environmentally-responsive, color-responsive

[a]*Faculty of Biotechnology, Chemistry and Environmental Engineering, Phenikaa University, Hanoi 12116, Vietnam. E-mail: tan.tranvan@phenikaa-uni.edu.vn*

[b]*Department of Chemistry, Chemical Engineering and Applied Chemistry, Chungnam National University, Daejeon, 34134, Republic of Korea*

[c]*Phenikaa University Nano Institute (PHENA), PHENIKAA University, Hanoi 12116, Vietnam. E-mail: tuan.hoangvan@phenikaa-uni.edu.vn; tuan.leanh@phenikaa-uni.edu.vn*

† Electronic supplementary information (ESI) available. See DOI: https://doi.org/10.1039/d3ra06754h

materials have recently drawn considerable attention, specifically in ion detection and monitoring applications.[9,17–19] PCs are structures that possess a periodic dielectric constant in one, two, or all three dimensions. They interact with light in unique ways due to their periodic nanostructure and can influence the propagation of electromagnetic waves, leading to the phenomenon of structural color. Several approaches used include direct adsorption/desorption causing RI and color change,[20] ion-responsive polymers causing structural change,[21] incorporation in microfluidic systems for fluidic ion detection,[22] and integration with field-effect transistors for electronic colorimetric sensing.[23] Furthermore, coupling with plasmonic nanoparticles enhances the optical response and sensitivity of the PC-based sensors.[24] While these methods have unlocked myriad detection capabilities, challenges remain in improving their sensitivity, selectivity, response time, and stability in diverse environmental conditions. Particularly, paper-based colorimetric sensors offer distinct advantages over traditional solution-based counterparts, primarily in terms of cost-effectiveness, ease of use, and portability.[25] These sensors are highly suitable for field tests and point-of-care applications, especially in resource-limited settings. Their capability to provide rapid, visually observable detection reduces the need for specialized equipment and extensive training. Moreover, the low sample volume requirement and environmental sustainability of these sensors, stemming from reduced waste generation, make them an appealing option. Although they may not achieve the sensitivity and quantitative accuracy of solution-based sensors, their accessibility and practicality in a variety of situations are invaluable, especially in contexts with limited resources.

Herein, we introduce for the first time a straightforward and unique colorimetric sensing platform for detection of Cl^-, employing MagPlas APAs as an exceptional colorimetric transducer. Upon introducing silver nitrate ($AgNO_3$) into this colloidal photonic network, the resulting array demonstrates excellent color responsiveness and can detect Cl^- with high selectivity, sensitivity, and stability. The simplicity, single-use nature, and uncomplicated structure of these devices present a compelling alternative to commonly used conventional methods.

2. Experimental

2.1. Preparation of MagPlas NPs

The Ag@Fe_3O_4 NPs were produced through a one-step solvothermal method, which involved the simultaneous reduction of $AgNO_3$ and iron nitrate ($Fe(NO_3)_3$) precursors in an ethylene glycol (EG) solution (refer to the ESI† for a detailed description of the synthesis procedure). The NPs were subsequently stabilized by a citric acid coating, which was applied *via* one or two carboxylate functionalities under moderate temperature conditions.

2.2. Fabrication of colorimetric sensors

Firstly, MagPlas APAs of Ag@Fe_3O_4 NPs was constructed on filter paper (polyethersulfone, GPWP04700, 0.22 μm pore size, Millipore Express) using an external magnetic field. Typically, a 20 μL drop of a 0.5 wt% colloidal solution was applied to a filter paper placed above a neodymium block magnet ($B = 800$ G). Once the droplet evaporated completely, the array was removed from the magnetic field and heated in an oven at 60 °C for 30 minutes. Cl^- sensors were subsequently fabricated by impregnating $AgNO_3$ into the fabricated APAs. For Cl^- detection, a 15 μL of sample was dropped onto the sensor surface, followed by drying at 60 °C for 3 minutes.

2.3. Characterization

The morphology of the Ag@Fe_3O_4 NPs was characterized by high-resolution transmission electron microscopy (HR-TEM, JEM-3010, Japan), field-emission scan electron microscopy (FE-SEM, S-4700, Hitachi, Japan). Magnetic measurements were performed using a superconducting quantum interference device (SQUID) magnetometer (MPMS XL-7, Quantum Design, Inc., San Diego, CA). The absorbance of NPs was carried out using UV-Vis spectroscopy (SCINCO, S310, Korea). Digital photographic images were obtained utilizing a Sony ILCE7RM2 camera. The reflectance spectra were assessed using a fiber-coupled spectrometer (Ocean Optics Inc., Flame), with a halogen lamp (DH-2000-BAL) serving as the light source.

3. Results and discussion

3.1. Characterization of Ag@Fe_3O_4 NPs

MagPlas NPs, consisting of Ag core and Fe_3O_4 shell (Ag@Fe_3O_4), were synthesized through a simple one-step solvothermal method, involving reduction reactions between Ag^+, Fe^{3+}, and EG, with their stabilization achieved by adsorbing citric acid.[26] The composition and structure of the NPs were ascertained through SEM, high-resolution transmission electron microscopy (HR-TEM), and UV-Vis spectroscopy. The SEM and HR-TEM images exhibit typical Ag@Fe_3O_4 NPs with an external diameter (d) of 175 ± 11 nm and a core diameter (d_{core}) of 55 ± 9 nm (Fig. S1a and b, ESI†). The detailed characterization of Ag@Fe_3O_4 NPs was conducted in our prior study, which definitively confirmed the composition and structure of these nanoparticles.[26] The zeta size distribution histogram confirms that the NPs are nearly monodispersed with a hydrodynamic size of ~190 nm (Fig. S1c†). The core–shell NPs display a consistent spherical morphology with quasi-spherical Ag cores that appear darker due to its higher electron density. The nomenclature NP_d and APA_d are utilized to denote the specific diameter of a MagPlas NP and its corresponding APA, respectively. For example, NP_{175} denotes a nanoparticle with a diameter of 175 nm. The Ag@Fe_3O_4 NPs, when dispersed in deionized water, display two unique extinction peaks at 417 nm and 699 nm, corresponding to the Fe_3O_4 shell and the Ag core, respectively (Fig. S1d†).[26] A pronounced extinction peak at 417 nm results from the Mie resonance light scattering effect, which is dominant due to the NPs' large diameter and the interband transitions of Fe_3O_4. Additionally, the shift of the Ag core's plasmon peak to 699 nm is due to the high RI of the dielectric medium.

3.2. Sensor design and optimization

Utilizing the novel magnetic properties of the NPs, a magnetic field-assisted coating technique was developed to fabricate closely packed arrays of Ag@Fe_3O_4 core–shell NPs, termed MagPlas APAs. Fig. S4† presents a representative SEM image of MagPlas APA, accompanied by its 2D fast Fourier transform displaying a circular pattern. This pattern suggests the presence of a well-defined short-range order, characteristic of an amorphous photonic structure. In our previous research, we demonstrated that MagPlas APAs possessed exceptional RI sensitivity and exhibited a swift color response to alterations in the surrounding dielectric constants.[26] Using this property, we designed a sensing system for Cl^- detection based on the interaction between Ag^+ and Cl^-, which results in the formation of high-RI silver chloride (AgCl). Given the inherent porosity of the photonic array structure, the precipitation formation within the array escalates the effective RI, inducing a color shift to a longer wavelength (λ). The design of the Cl^- sensor is illustrated in Scheme 1, highlighting the crucial role of the impregnation substance, $AgNO_3$. With this sensing platform, the appropriate choice of an impregnation substance can facilitate the detection of a specific analyte.

It was observed that MagPlas NPs of varying sizes manifested dissimilar color response characteristics in their APAs upon water absorption. Consequently, to identify the optimal NPs for the fabrication of sensors, we studied the color response behavior of APAs to Cl^- utilizing Ag@Fe_3O_4 NPs of five different sizes. The size and morphology of different Ag@Fe_3O_4 NPs are depicted in Fig. S2 and S3.† Fig. 1a–e illustrate that all photonic films, in the absence of added Cl^-, display one reflectance dip and two main reflectance peaks at the short- and long-wavelength ranges. It is evident that the color changes of four samples are barely noticeable, with the exception of APA_{184}, which changes from a royal purple to a dark sky blue hue. As shown in the reflectance spectra, the remaining four samples display minimal redshifts of the reflectance dip and the long-wavelength peak, but the short-wavelength peak remains unchanged. In contrast, APA_{184} exhibits significant shifts across all peaks and dip. The reflectance dip was chosen as a representative measure to compare the spectral changes of photonic films after addition of Cl^- (Fig. 1f). The shift in APA_{184}'s reflectance dip is remarkably notable, being 2 to 6 times greater than the shifts observed in other samples.

A distinct variation in color response behavior of APAs has been noted when interacting with Cl^- as opposed to water. The spectral shifts of APAs after wetting are depicted in Fig. S5,† highlighting an enhanced color response capability corresponding to an increase in MagPlas NP size from 150–200 nm. Notably, APA_{234P}, comprised of porous NP_{234}, demonstrates a substantial reflectance shift in comparison to other APAs. In this scenario, water molecules can readily infiltrate both the magnetic nanoparticle (NP) shell and the colloidal photonic structure voids *via* diffusion, leading to alterations in the local RI with subsequent impact on both photonic and plasmonic properties.[27,28] The photonic response is governed by the total loading capacity of water molecules, which is determined by particle porosity and packing regimen. Concurrently, the Ag core diameter (d_{core}) emerges as a crucial factor influencing the plasmonic response, due to size-dependent sensitivity of short- and long-range plasmonic effects.[29,30] As established in our preceding research, a distinct correlation has been observed between the concentration of Fe^{3+} and the dimensions of certain structural elements. Specifically, the external diameter, the radius of the Ag core, and the thickness of the Fe_3O_4 shell (t_{shell}) have all been observed to incrementally rise in direct response to an increase in Fe^{3+} concentration. As such, smaller NPs, with their reduced core size and lower t_{shell}-to-d_{core} ratio, can be anticipated to exhibit a diminished color response relative to larger particles. This can be attributed to a dual factor: decreased plasmonic sensitivity and reduced water molecule loading capacity. For APA_{234P}, a larger d_{core}, a higher t_{shell}-to-d_{core} core ratio, and a highly porous shell resulting from the etching process work together to enhance the color response of the photonic film. In contrast, when focusing on Cl^- sensing, the situation diverges due to the RI change being a consequence of the formation of the AgCl precipitate. Since this precipitate is solid with limited diffusion into the particle shell, the color response of a Cl^- sensor is predominantly dictated by the volume of the voids and the Ag core's long-range plasmonic sensitivity.[31,32]

3.3. Sensitivity test

Utilizing the optimally-selected NPs, a comprehensive investigation was performed on the sensing capabilities of the proposed platform, encompassing sensitivity, selectivity, and resistance to interference. The sensitivity of the platform was evaluated by modulating the concentration of impregnated $AgNO_3$ (C_{AgNO_3}), a key determinant of the maximum AgCl production, as well as potential chromatic change. With a concentration of 50 mM $AgNO_3$, the sensor exhibited negligible color variation until C_{Cl} reached a level of 0.25 mM, at which point a faint, thin blue ring emerged (Fig. S6a†). This ring increased in visibility, thickness, and reduced in diameter as C_{Cl} levels increase to 1.5 mM. Increasing C_{Cl} to 2 and 5 mM transformed the ring into a uniform disc, with the most prominent wavelength shift occurring at 5 mM (Fig. S6b and c†). Intriguingly, neither the ring nor disc was discernible when C_{Cl} was elevated to or beyond 7.5 mM. The data suggests that the sensor offers limited visual discernment and a detection range of 0.25–5 mM at a C_{AgNO_3} of 50 mM. When the C_{AgNO_3} was elevated to 100 mM, the color transformation became faintly perceivable at a C_{Cl} of 0.1 mM, achieving complete clarity at 0.5 mM. The blue ring rapidly converted into a uniform disc as C_{Cl} levels surged above 1 mM (Fig. S7a†). The maximum color change was realized at 5 mM, but any subsequent increase in C_{Cl} led to a decrease in color change (Fig. S7b and c†). Importantly, the disc diminishes significantly but doesn't disappear entirely at C_{Cl} levels of 7.5 mM or higher, suggesting a low visualization capacity of the sensor at elevated C_{Cl} levels. At C_{AgNO_3} of 250 and 500 mM, the color shift behavior mirrored that of C_{AgNO_3} at 100 mM when C_{Cl} was at a lower concentration (Fig. 2a and S8a†). However, at elevated C_{Cl} levels, the

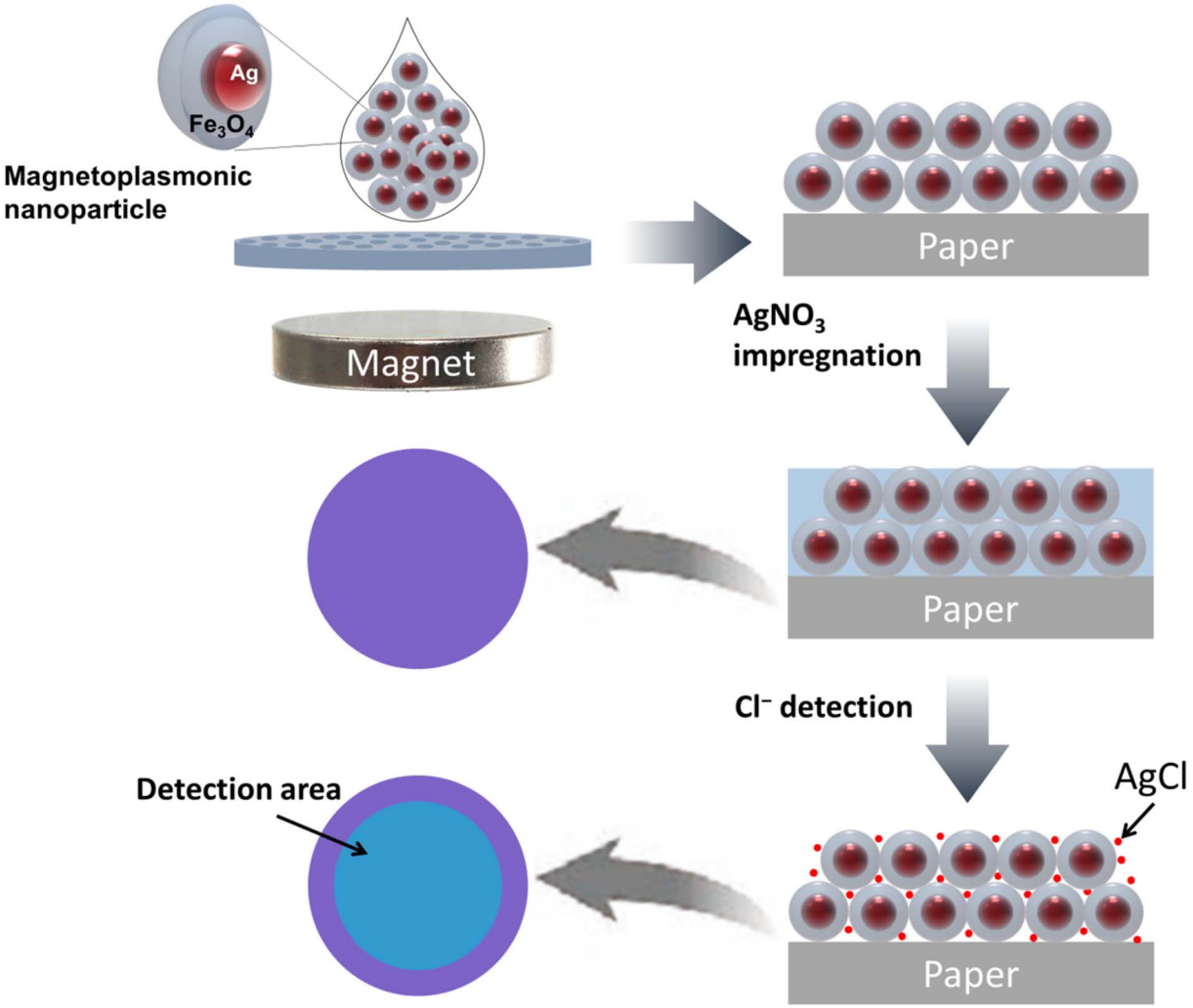

Scheme 1 Schematic illustration of Cl^- sensor fabrication.

wavelength shift demonstrated a consistent rise, and the disc preserved its size and robust color visibility as C_{Cl} increased (Fig. 2b, c, S8b and c†). It's worth highlighting that a saturation point in the wavelength shift was observed at $C_{Cl} \geq 5$ mM for C_{AgNO_3} at 500 mM, whereas the sensor with C_{AgNO_3} at 250 mM demonstrated no such saturation indications. The estimated best Limit of Detection (LOD) for the sensor was 0.233 mM, within a detection range of 0.5–5 mM, for the sensor impregnated with 500 mM $AgNO_3$. However, due to its extensive linear detection range and consistent performance, we opted for the sensor impregnated with 250 mM $AgNO_3$ for further testing.

3.4. Selectivity test

To assess the selectivity profile of the sensor, we examined various chloride salts with different cation species, including Mg^{2+}, Ni^{2+}, NH_4^+, Zn^{2+}, Co^{2+}, Ba^{2+} and Sr^{2+} each at a concentration of 5 mM. The results of this examination revealed that the sensor similar color change behavior to all chloride salts (Fig. 3a), indicating no significant interfered from these tested cations. Subsequently, we expanded our analysis to include other anions (F^-, SO_4^{2-}, NO_2^-, and NO_3^-). It should be noted that these concentrations significantly exceed those typically found in water samples. It is apparent that the sensor did not exhibit any noticeable color changes when exposed to any of the tested species. It is important to highlight that the formation of precipitates also occurs in cases involving F^- and NO_2^- ions. However, no discernible color change was observed in these scenarios, which can be attributed to the lower RI of the resultant precipitates, namely silver fluoride (AgF) and silver nitrite ($AgNO_2$). Additionally, the solubility of these two salts are significantly higher than that of AgCl, leading to amount of precipitate of AgF is so small that it could not induce the color change. The response of sensor to Br^- and I^- was also examined, indicating that similar color change compared to Cl^- was observed (Fig. S9†). This observation aligns with the comparable solubility and refractive indices of these silver halides. Consequently, for the effective application of this detection method, a pretreatment process is necessary to remove Br^- and I^- prior to detection. Furthermore, we quantified the mean color

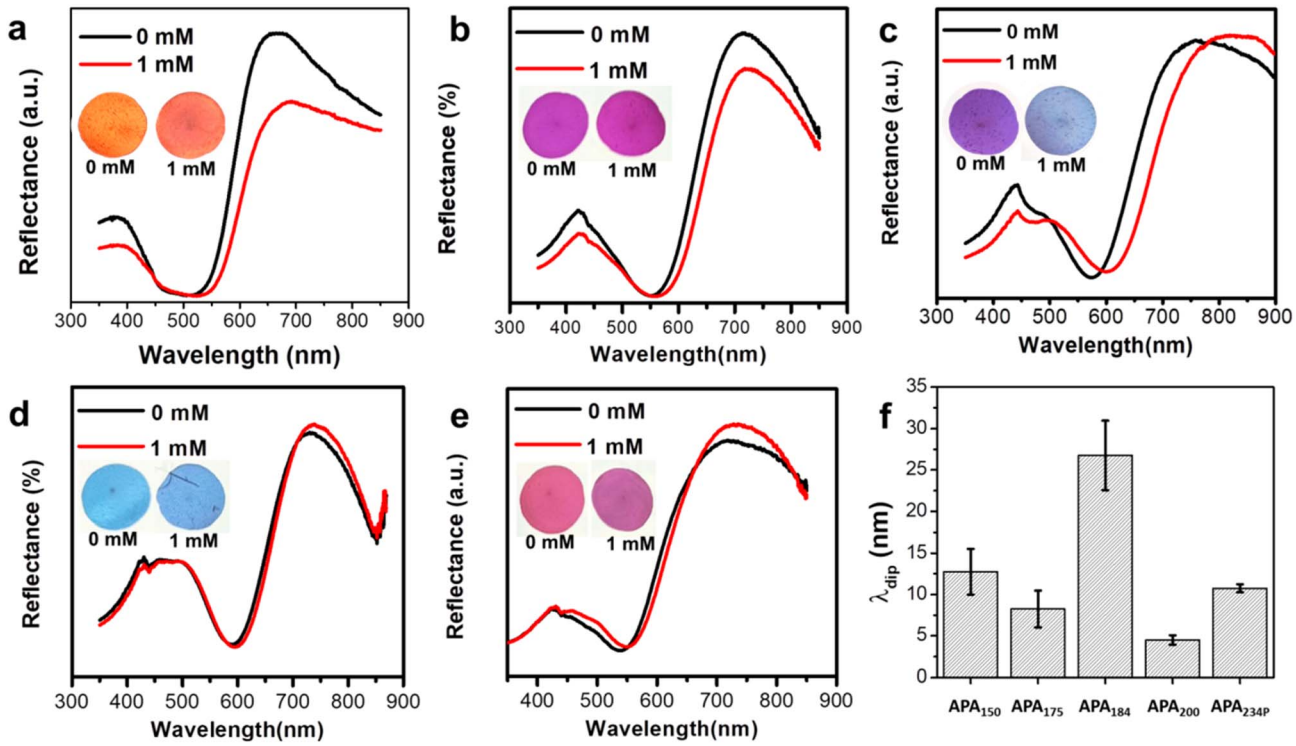

Fig. 1 Reflectance spectra and photographs (inset) of MagPlas APAs composed of different NPs: (a) 150 nm, (b) 175 nm, (c) 184 nm, (d) 200 nm, and (e) porous 234 nm. (f) The wavelength shifts of reflectance dip upon adding 1 mM NaCl.

difference ($\Delta\lambda = \lambda_{\text{tested species}} - \lambda_{\text{blank}}$) between the tested species and the control. The analysis verifies that only Cl^- were found to cause significant wavelength shifts of the photonic film, as depicted in Fig. 3b. Consequently, this proposed sensor exhibits good selectivity, making it suitable for use in real-world sample analysis.

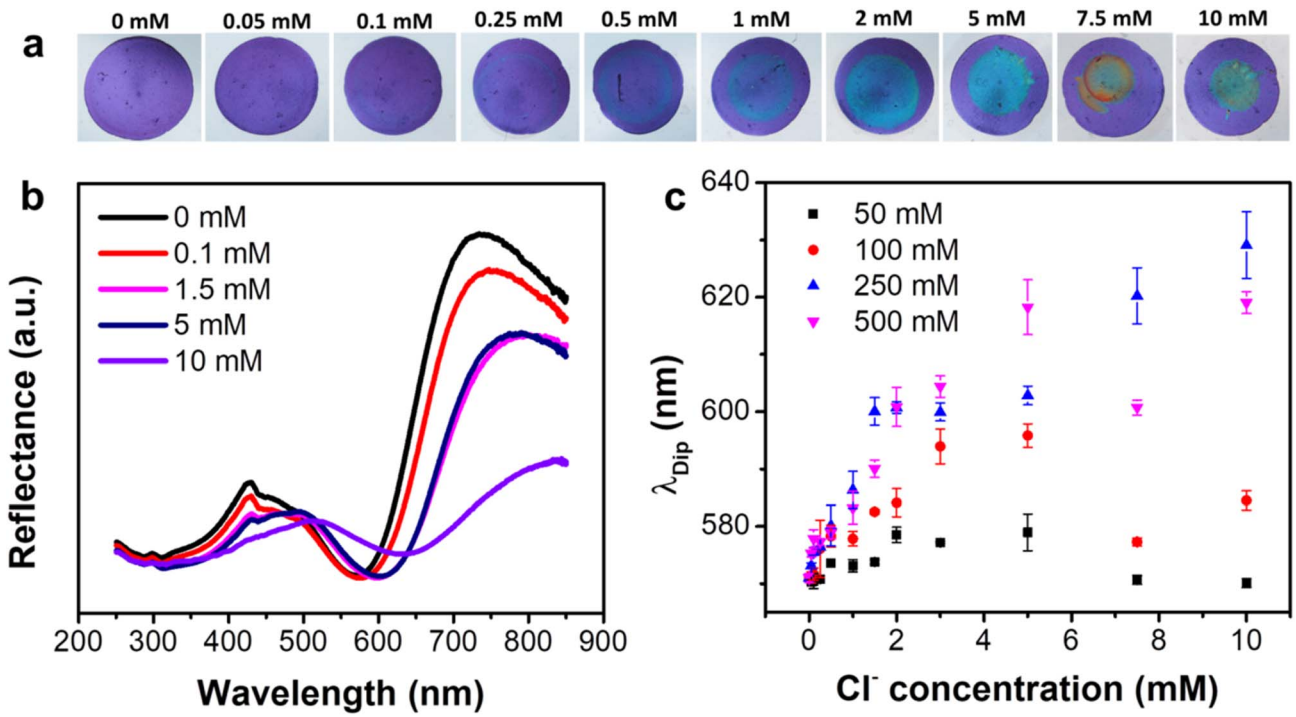

Fig. 2 (a) Photographs and (b) reflectance spectra of MagPlas APA_{184} impregnated with 250 mM $AgNO_3$ after adding solutions with different C_{Cl}. (c) The dependence of λ_{dip} on C_{Cl} of MagPlas APA_{184} impregnated with different C_{AgNO_3}.

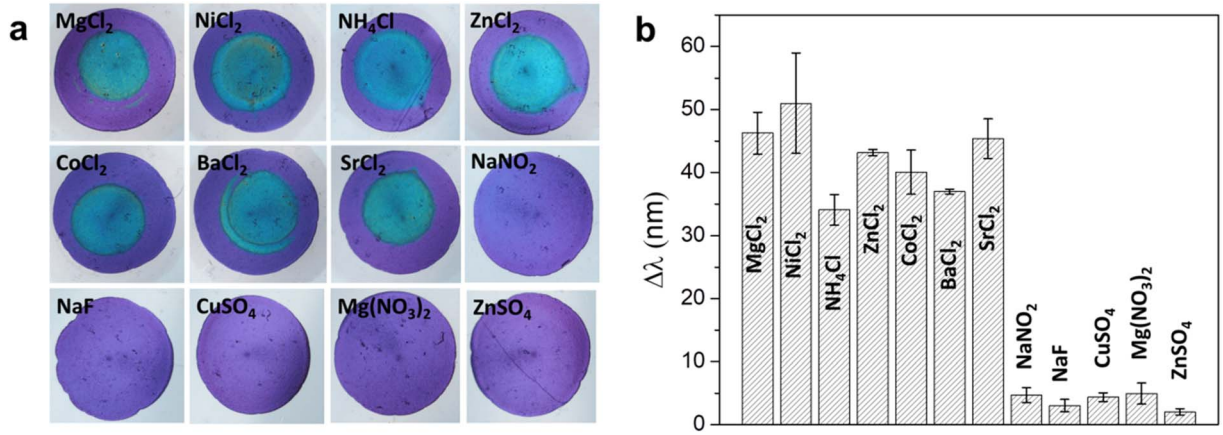

Fig. 3 (a) Photographs and (b) the wavelength shifts of reflectance dip of MagPlas APA_{184} impregnated with 250 mM $AgNO_3$ after adding 5 mM solution of different salts.

3.5. Stability and real sample test

In order to substantiate the results, a mixture of potential interfering species was tested at a concentration of 5 mM in conjunction with an equivalent concentration of Cl^- using the proposed sensors. The results obtained from testing the mixture solution were insignificantly different from those derived from the sole Cl^- tests, as depicted in Fig. 4. Consequently, it can be confidently stated that this sensor demonstrates a high degree of selectivity and robustness towards Cl^- detection. Besides, we have performed additional stability testing one week post sample injection. The results demonstrate that the sensor's color remains nearly unchanged when stored under normal room conditions, confirming the stability and consistency of the sensor's readout for extended monitoring (Fig. S10†). This finding is in line with our previous work, which also highlighted the high color stability and robustness of the APA across 50 wetting–drying cycles.[26]

To authenticate the utility of the sensor, an array of local water samples was tested, including tap water, reverse osmosis (RO) water, and rainwater (Fig. 5). The data reveals that tap water sources contain relatively high concentration of Cl^-. Interestingly, the Cl^- content in rainwater is also detectable by the sensor, which usually comes from sea spray and human activities such as combustion of fossil fuels/

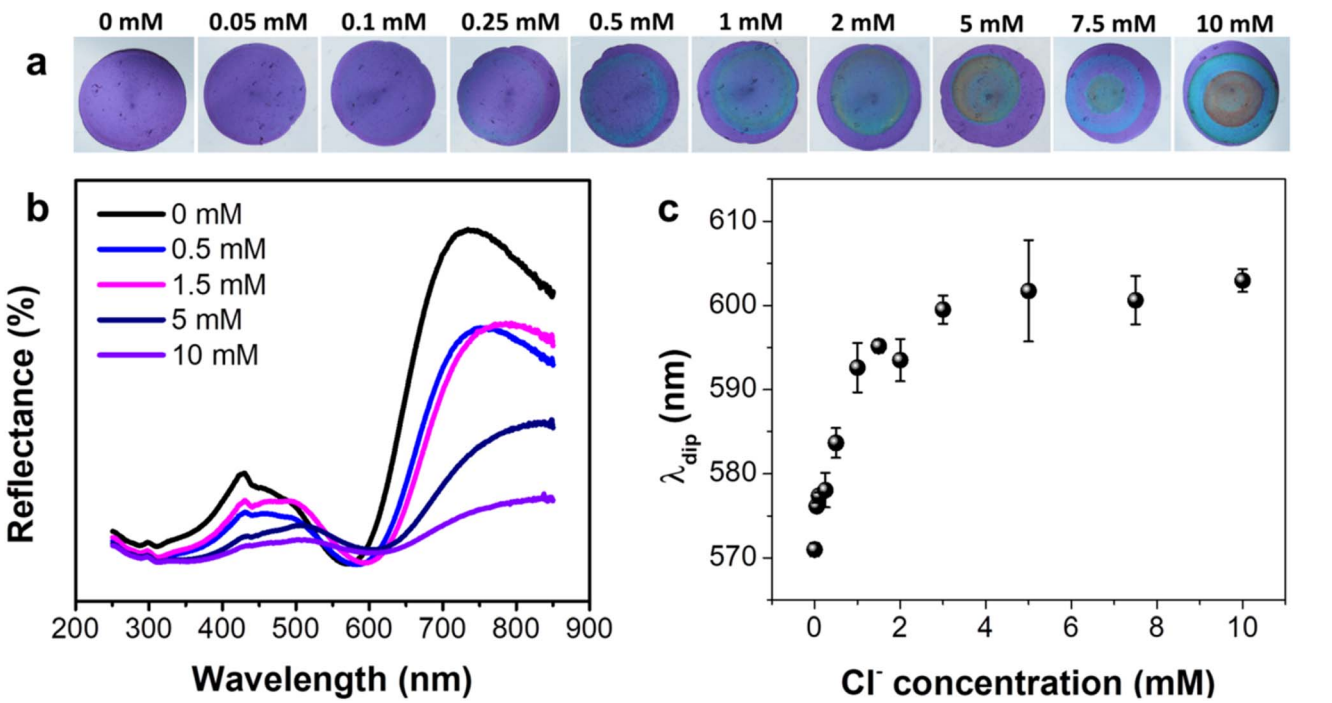

Fig. 4 (a) Photographs and (b) reflectance spectra of photonic arrays impregnated with 250 mM $AgNO_3$ after adding solutions with different C_{Cl} mixed with salts: $Mg(NO_3)_2$, $CuSO_4$, and NaF (5 mM). (c) The dependence of λ_{dip} on C_{Cl}.

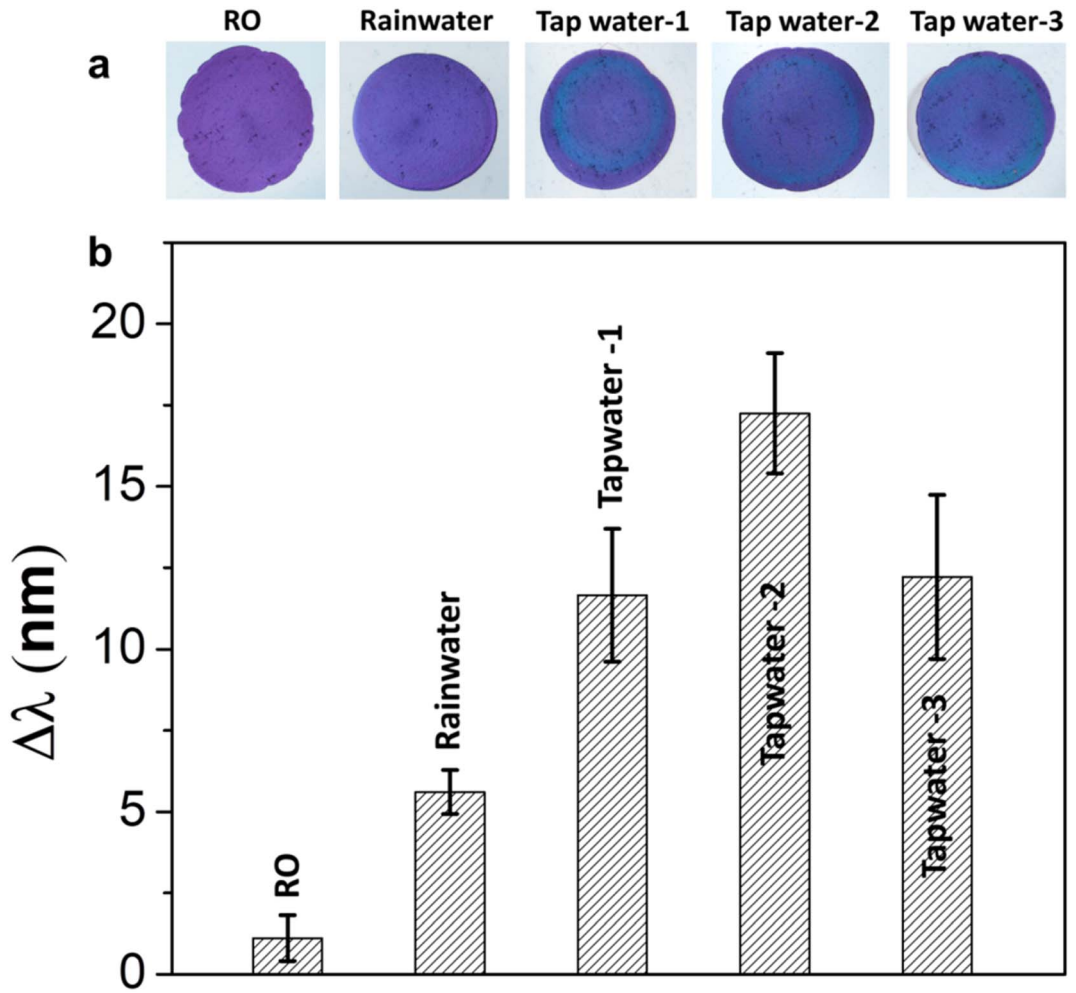

Fig. 5 (a) Photographs and (b) peak shifts of photonic arrays impregnated with 250 mM $AgNO_3$ before adding real samples (without any diluting).

biomass and industrial processes. Meanwhile, the RO water shows undetectable level of Cl^-, aligning with the reported parameters for commercial water purifiers.[33] These outcomes suggest that the colorimetric sensor developed in this study has the potential for reliable determination of Cl^- in real natural water samples.

4. Conclusion

Leveraging the unique optical characteristics of the MagPlas photonic array, we have successfully developed a paper-based colorimetric methodology for the detection of Cl^-. Under ideal conditions, this colorimetric sensor demonstrated commendable selectivity towards Cl^-, as opposed to other environmentally relevant species. Additionally, this proposed method was successfully implemented for the detection of Cl^- levels in real water samples. This process necessitates no surface modification and open up ability to detect various anions species by changing impregnated salts. Due to its versatility and simplicity, this colorimetric sensor holds promise for on-site determination and screening of ions in both environmental and biomedical contexts.

Author contributions

V. T. Tran: conceptualization, formal analysis, writing – original draft; V. D. Dao: formal analysis, writing-review & editing; H. Q. Nguyen: investigation, data curation; L. T. Tufa: investigation; writing – review & editing; J. Lee: methodology, formal analysis; V. T. Hoang: conceptualization, formal analysis, writing – original draft; A. T. Le: conceptualization, methodology, writing – review & editing.

Conflicts of interest

The authors declare that they have no known competing financial interests or personal relationships that could have appeared to influence the work reported in this paper.

Acknowledgements

This research was supported by the Phenikaa University under grant number 2-04.2021.03. The authors would like to acknowledge the experimental supports from NEB Lab

(Phenikaa University), and SEM, TEM characterizations from Chungnam National University-South Korea.

References

1 S. Bolisetty and R. Mezzenga, *Nat. Nanotechnol.*, 2016, **11**, 365–371.
2 L. McCallum, S. Lip and S. Padmanabhan, *Pflug. Arch. Eur. J. Physiol.*, 2015, **467**, 595–603.
3 A. Koh, D. Kang, Y. Xue, S. Lee, R. M. Pielak, J. Kim, T. Hwang, S. Min, A. Banks and P. Bastien, *Sci. Transl. Med.*, 2016, **8**, 366ra165.
4 K. W. Edgell, J. E. Longbottom and J. D. Pfaff, *J. AOAC Int.*, 1994, **77**, 1253–1263.
5 A. Bratovcic and A. Odobasic, in *Environmental Monitoring*, IntechOpen, 2011, pp. 109–120.
6 D. L. Rocha and F. R. Rocha, *Microchem. J.*, 2013, **108**, 193–197.
7 F. E. Clarke, *Anal. Chem.*, 1950, **22**, 553–555.
8 W. Horwitz, *Official Methods of Analysis of Aoac International (Oma)*, Gaithersburg, 2000.
9 V. T. Tran, H. Q. Nguyen, Y. M. Kim, G. Ok and J. Lee, *Nanomaterials*, 2020, **10**, 2248.
10 J. Hou, M. Li and Y. Song, *Nano Today*, 2018, **22**, 132–144.
11 J. N. Anker, W. P. Hall, O. Lyandres, N. C. Shah, J. Zhao and R. P. Van Duyne, *Nat. Mater.*, 2008, **7**, 442–453.
12 L. Guo, J. A. Jackman, H. H. Yang, P. Chen, N. J. Cho and D. H. Kim, *Nano Today*, 2015, **10**, 213–239.
13 Y. Xu, P. Bai, X. Zhou, Y. Akimov, C. E. Png, L. Ang, W. Knoll and L. Wu, *Adv. Opt. Mater.*, 2019, **7**, 1801433.
14 B. Liu, J. Zhuang and G. Wei, *Environ. Sci.: Nano*, 2020, **7**, 2195–2213.
15 D. Vilela, M. C. Gonzáslez and A. Escarpa, *Anal. Chim. Acta*, 2012, **751**, 24–43.
16 V. N. Mehta, N. Ghinaiya, J. V. Rohit, R. K. Singhal, H. Basu and S. K. Kailasa, *TrAC, Trends Anal. Chem.*, 2022, **153**, 116607.
17 A. K. Yetisen, Y. Montelongo, M. M. Qasim, H. Butt, T. D. Wilkinson, M. J. Monteiro and S. H. Yun, *Anal. Chem.*, 2015, **87**, 5101–5108.
18 H. Inan, M. Poyraz, F. Inci, M. A. Lifson, M. Baday, B. T. Cunningham and U. Demirci, *Chem. Soc. Rev.*, 2017, **46**, 366–388.
19 X. Hou, F. Li, Y. Song and M. Li, *J. Phys. Chem. Lett.*, 2022, **13**, 2885–2900.
20 X. Qiu, Y. Li, D. Liu, K. Zhou, Y. Wang and H. Guo, *Spectrochim. Acta, Part A*, 2022, **283**, 121719.
21 E. P. Van Heeswijk, A. J. Kragt, N. Grossiord and A. P. Schenning, *Chem. Commun.*, 2019, **55**, 2880–2891.
22 P. S. Nunes, N. A. Mortensen, J. r. P. Kutter and K. B. Mogensen, *Opt. Lett.*, 2008, **33**, 1623–1625.
23 Y. Cho, V. A. Pham Ba, J. Y. Jeong, Y. Choi and S. Hong, *Sensors*, 2020, **20**, 3680.
24 B. Yu, F. Zhai, H. Cong and D. Yang, *J. Mater. Chem. C*, 2016, **4**, 1386–1391.
25 H. Jang, J. H. Park, J. Oh, K. Kim and M. G. Kim, *ACS Sens.*, 2019, **4**, 1103–1108.
26 V. T. Tran, J. Kim, S. Oh, K.-J. Jeong and J. Lee, *Small*, 2022, **18**, 2200317.
27 J. Wang, S. Ahl, Q. Li, M. Kreiter, T. Neumann, K. Burkert, W. Knoll and U. Jonas, *J. Mater. Chem.*, 2008, **18**, 981–988.
28 K. Yu, T. Fan, S. Lou and D. Zhang, *Prog. Mater. Sci.*, 2013, **58**, 825–873.
29 S. Szunerits, M. R. Das and R. Boukherroub, *J. Phys. Chem. C*, 2008, **112**, 8239–8243.
30 O. Kedem, A. B. Tesler, A. Vaskevich and I. Rubinstein, *ACS Nano*, 2011, **5**, 748–760.
31 E. Galopin, A. Noual, J. Niedziólka-Jönsson, M. Jönsson-Niedziólka, A. Akjouj, Y. Pennec, B. Djafari-Rouhani, R. Boukherroub and S. Szunerits, *J. Phys. Chem. C*, 2009, **113**, 15921–15927.
32 X. Wang, P. Gogol, E. Cambril and B. Palpant, *J. Phys. Chem. C*, 2012, **116**, 24741–24747.
33 J. Cotruvo, *Drinking water quality and contaminants guidebook*, CRC Press, 2018.